Supporting Information

Yuthavong et al. 10.1073/pnas.1204556109

SI Text

SI Results and Discussion. ***P218 binding to Plasmodium falciparum and human dihydrofolate reductase (DHFRs).*** P218 and P65 bind to quadruple mutant *P. falciparum* (Pf) DHFR with their respective phenyl rings coplanar but shifted in plane by about 1.4 Å in a direction that moves the phenyl ring of P218 closer to the extended side chain of Arg122 (Fig. S2*B*). One face of the P218 phenyl ring makes extensive van der Waals contacts with the side chains of Ile112 and Pro113 whereas the side chain of Phe116 has edge-on interactions with the inhibitor's phenyl ring and its carboxyethyl substituent (Fig. S2*C*). The side chain of Leu119 also is in van der Waals contact with the inhibitor's ethyl group. The flexible side chain of Met55 moves about 4 Å from its position in the cocrystal structure with dihydrofolate to a new location underneath the phenyl of P218, where it also contacts hydrophobic portions of the carboxyethyl moiety, as does the side chain of conserved Phe58 (Fig. S2*C*). The very short in-line approach of a Phe58 aromatic side-chain CH to one of the P218 carboxylate oxygens (3.1 Å) indicates a hydrogen bond between the two (Fig. S2*C*). Together, these interactions stabilize a binding mode for the carboxyethylphenyl of P218 in which its fully extended ethyl side chain optimally positions the carboxylate for interaction with Arg122. Two parallel charge-mediated hydrogen bonds form between the inhibitor's carboxylate and side-chain amidine nitrogens of Arg122. One of the carboxylate oxygens has additional tetrahedrally disposed hydrogen-bonding interactions with the side chain of Arg59 and with an ordered water molecule.

P218 binds differently to human DHFR and does not form hydrogen bonds with the conserved active-site Arg as seen in the complex with quadruple mutant (QM) PfDHFR (Figs. 3 and S2*D*). Upon binding P218, the side chain of Phe31, as positioned in the human DHFR folate complex, rotates 120 degrees about its Cα—Cβ bond into a new position at the back of the substrate binding site near Arg70 (Fig. S2*D*). This change is associated with a major repositioning of the inhibitor's carboxyethylphenyl group relative to that seen in quadruple mutant PfDHFR such that the carboxylate moves into the area vacated by the side chain of Phe31, where it is hydrated by an ordered water molecule and interactions with bulk solvent (Fig. S2*D*).

To understand why P218 binds differently to human DHFR despite the presence in all DHFRs of conserved Arg122, we aligned the human DHFR cocrystal structure containing bound folate [Protein Data Bank (PDB) ID code 2W3M] to the quadruple mutant PfDHFR structure with P218 to assess how P218 in its mutant PfDHFR–binding mode would interact with hDHFR (Fig. S2*D*). The flexible side chain of Met55 in quadruple mutant PfDHFR-TS undergoes a large conformational change upon binding P218, and in its new position creates favorable van der Waals contacts underneath the inhibitor's phenyl ring and its carboxyethyl substituent. Met55 in quadruple mutant PfDHFR is replaced in human DHFR by the more conformationally constrained Phe31. If P218 bound to human DHFR in a similar manner as it does to quadruple mutant PfDHFR, the Phe31 side chain would be positioned significantly off to one side (as it is in the human DHFR-folate cocrystal structure), and not in direct contact with the inhibitor's carboxyethylphenyl group (see Fig. S2*D*). Phe31 would be too far away for direct van der Waals contact with all but one carbon of the benzene ring, and at its closest approach would be 5 Å from any portion of the carboxyethyl group. Phe side chains have three well-defined potential energy minima for rotation about the Cα—Cβ bond. The other two energetically allowed conformers for Phe31 in human DHFR would either move the side chain out into bulk solvent or sterically block binding of P218 in the orientation seen in Fig. S2*D* for its binding to quadruple mutant PfDHFR-TS. On the opposite face of the carboxyethylphenyl, the side chain of Asn64 (structurally equivalent to Phe116 in PfDHFR) is too far away and too polar to provide the important hydrophobic interactions that, for PfDHFR, assist in orienting the carboxyethylphenyl group for interaction with the conserved Arg.

In summary, important but nonconserved active-site amino acids responsible for binding and orienting the carboxyethylphenyl of P218 in PfDHFR for interaction with Arg122, namely Met55 and Phe116, are replaced in the human enzyme at structurally equivalent positions with different amino acids (Phe31 and Asn64) that cannot function similarly, resulting in distinctly different binding modes for P218 in the two enzymes. A diagram showing some interactions of P218 with active-site residues of the quadruple mutant PfDHFR is shown in Fig. S2*E*.

Results of the exploratory safety studies. P218 had no effect of hERG-mediated tail current at concentrations up to 30 μM, with a minor effect (10% reduction in tail current) at 100 μM. In the rat toxicology study, there were no mortalities in any group. Salivation after the administration was recorded in three animals from group 2 (100 mg/kg/*d*) and in all animals from group 3 (300 mg/kg/*d*). On the last day of the recovery period, abnormal gait was observed in the two animals from group 3, along with hunched back and ruffled fur in one of them. During the treatment period, lower food consumption was observed in group 3. During the recovery period, group 3 food consumption was still lower compared to the control group. No relevant differences were observed in group 2.

Lower body weight and body-weight gain were observed in animals from group 3 during the treatment period compared to the control group. During the recovery period, a decrease in body weight and body-weight gain was observed in this group; however, no relevant differences were observed in group 2. In the hematological analyses, lower absolute and relative reticulocyte counts were observed at the end of treatment in groups 2 and 3 compared to the control group. Higher absolute and relative neutrophil counts with respect to those recorded in the control group were also observed in group 3. At the end of the recovery period, differences in the reticulocyte and neutrophil counts were still observed for group 3. No relevant differences between group 2 and control group were observed at the end of the recovery period. In the biochemical analyses, lower triglyceride and calcium values compared to the control group were recorded in groups 2 and 3. Higher glucose levels were also recorded in group 3. At the end of the recovery period, no relevant differences were observed between test item–treated groups and control group. No relevant differences were recorded in the urinalysis in groups 2 or 3, and blood biochemistry changes were not marked. At the end of the treatment period, a trend toward lower thyroid weights was observed in groups 2 and 3. Higher weight of the kidneys and lower weight of the spleen were recorded in animals from group 3. However, differences were only statistically significant in the case of the relative weight of the kidneys. No relevant differences were observed at the end of the recovery period. Macroscopic alterations related to treatment with the test item seemed to be present in group 3, and consisted of stomach with whitish mucosa and reddish discoloration or reddish area in cecum. Other changes were within the range of normal background findings in rats of this strain and age. In view of the results obtained, the no

observed adverse effect level (NOAEL) was determined to be approximately 100 mg/kg/*d* for the oral administration of P218 to rats over a 5-*d* period.

SI Materials and Methods. ***Synthetic aspects.*** All reagents were distilled before use. *N*, *N*-dimethylformamide (DMF) was dried over CaH_2 and distilled before use. Melting points were measured using an Electrothermal IA9100 digital melting-point apparatus and were uncorrected. NMR spectra were recorded on Bruker DRX 400-MHz spectrometer. Electrospray ionization time-of-flight MS data were measured with a Bruker MicroToF mass spectrometer.

Synthesis of 2,4-diamino-6-methyl-5-[3′-(2,4,5-trichlorophenoxy) propyloxy]-pyrimidine (P65). Synthesis of 3-(2,4,5-trichlorophenoxy) propyl bromide. Sodium hydride (607.7 mg, 25.32 mmol, 1 equivalent) was slowly added to a suspension of 2,4,5-trichlorophenol (5 g, 25.32 mmol, 1 equivalent) in dry DMF (25 mL) at 0 °C under nitrogen and left stirring at 0 °C for 1 h. This reaction mixture was heated to 80 °C with vigorous stirring, then 1,3-dibromopropane (12.9 mL, 126.6 mmol, 5 equivalents) was added in one portion. The reaction mixture was stirred at this temperature for a further 10 min. After quenching with water at 0 °C, the solution was extracted three times with dichloromethane (3 × 100 mL). The combined extracts were dried over $MgSO_4$ and the solvents removed by rotary evaporation. Purification by silica gel column chromatography using 10% EtOAc/hexanes as the eluent gave the desired product, which was further purified by crystallization from a mixture of dichloromethane and hexanes to afford a white solid (4.43 g, 55% yield, mp = 49.2–49.5 °C) (1); ^{1}H NMR (400 MHz, $CDCl_3$) δ: 2.37 (m, 2H), 3.64 (t, J = 6.3 Hz, 2H), 4.15 (t, J = 6.3 Hz, 2H), 7.02 (s, 1H), 7.45 (s, 1H) ppm.

2,4-Diamino-6-methyl-5-[3′-(2,4,5-trichlorophenoxy)propyloxy]pyrimidine (P65). 2,4-Diamino-6-methyl-5-hydroxypyrimidine (700.7 mg, 5 mmol) was added to a stirring mixture of lithium hydroxide monohydrate (629.4 mg, 15 mmol, 3 equivalents) in DMF (4 mL), and the reaction was stirred at room temperature for 1 h. A solution of 3-(2,4,5-trichlorophenoxy)propyl bromide (1.59 g, 5 mmol, 1 equivalent) in DMF (1 mL) was added, and the reaction mixture was stirred at room temperature overnight. The DMF was partially removed under reduced pressure to give a residue, which was diluted with water (50 mL) followed by extraction with dichloromethane (3 × 100 mL), drying, and evaporation to dryness under reduced pressure. Purification by silica gel column chromatography using 8% MeOH/CH_2Cl_2 as the eluent gave the desired product. Crystallization from dioxane–methanol afforded a white solid (1.23 g, 65% yield, mp 159–160 °C); ^{1}H NMR (400 MHz, DMSO-d_6) δ: 1.98 (s, 3H), 2.16 (m, 2H), 3.77 (t, J = 6 Hz, 2H), 4.29 (t, J = 6 Hz, 2H), 5.58 (s, 2H), 6.11 (s, 2H), 7.52 (s, 1H), 7.81 (s, 1H); ^{13}C NMR (100 MHz, DMSO-d_6) δ: 17.9, 29.4, 66.9, 68.5, 115.9, 121.7, 123.1, 129.3, 130.9, 131.0, 153.9, 155.6, 158.5, 159.3 ppm. High-resolution electrospray ionization MS (HR-ESI-MS) calculated for $C_{14}H_{16}Cl_3N_4O_2(M+H)^+$: 377.0339, found: 377.0217.

2,4-Diamino-6-ethyl-5-(3-(2-(2-carboxyethyl)phenoxy)propoxy)pyrimidine hydrochloride (P218). Methyl 3-(2-hydroxyphenyl)propanoate. To a stirred solution of dihydrocoumarin (10 mL, 78.9 mmol) in dry methanol (200 mL), 500 microliters of concentrated sulfuric acid were added, and the reaction mixture was then stirred at 45 °C for 8 h under nitrogen. Evaporation under reduced pressure gave a residue, which was neutralized with anhydrous potassium carbonate at 0 °C. After neutralization, the oily residue was diluted with CH_2Cl_2 (200 mL) and washed with water (50 mL). The dichloromethane layer was dried (Na_2SO_4) and evaporated under reduced pressure to afford a light-yellow oil. Crystallization from hexanes at 0 °C gave the desired ester as a white solid (12.09 g, 85% yield, mp = 40–41 °C); ^{1}H NMR (400 MHz, $CDCl_3$) δ: 2.71 (t, J = 6.4 Hz, 2H), 2.89 (t, J = 6.4 Hz, 2H), 3.67 (s, 3H), 6.83–6.87 (m, 2H), 7.06–7.12 (m, 2H) ppm.

Methyl 3-(2-(3-bromopropoxy)phenyl)propanoate. To a solution of methyl 3-(2-hydroxyphenyl)propanoate (7.21 g, 40 mmol) and triphenylphosphine (12.59 g, 48 mmol, 1.2 equivalents) in dry THF (50 mL) was added diisopropyl azodicarboxylate (9.5 mL, 48 mmol, 1.2 equivalents) at 0 °C over 20 min under nitrogen. After 2 h at 0 °C, 3-bromo-1-propanol (4.4 mL, 48 mmol, 1.2 equivalents) was added dropwise, and the reaction was then left stirring at room temperature for 8 h. Evaporation of the THF yielded a yellow oil, which was suspended in water and extracted three times with CH_2Cl_2 (3 × 100 mL). The combined organic extracts were dried ($MgSO_4$), filtered, and concentrated to give the crude product, which was digested with hexanes. The white precipitate was discarded and the hexanes extract was evaporated to dryness. Purification by silica gel column chromatography (hexanes:CH_2Cl_2:EtOAc = 6.7:3:0.3 as the eluent) gave the title compound as a yellow oil (9.1 g, 75% yield) (2); ^{1}H NMR (400 MHz, $CDCl_3$) δ: 2.33 (m, 2H), 2.58 (t, J = 7.8 Hz, 2H), 2.92 (t, J = 7.8 Hz, 2H), 3.61 (t, J = 6.4 Hz, 2H), 3.65 (s, 3H), 4.10 (t, J = 5.7 Hz, 2H), 6.84 (d, J = 8.4 Hz, 1H), 6.88 (d, J = 7.3 Hz, 1H), 7.13–7.19 (m, 2H); ^{13}C NMR (100 MHz, $CDCl_3$) δ: 26.0, 30.1, 32.3, 34.1, 51.5, 65.0, 111.06, 120.7, 127.6, 128.8, 129.9, 156.3, 173.7 ppm.

2,4-Diamino-6-ethyl-5-(3-(2-(2-carboxyethyl)phenoxy)propoxy)pyrimidine (P218 free base). A suspension of 2,4-diamino-6-ethyl-5-hydroxypyrimidine (770.8 mg, 5 mmol) and lithium hydroxide monohydrate (629.4 mg, 15 mmol, 3 equivalents) in DMF (5 mL) was stirred at room temperature for 30 min. A solution of methyl 3-(2-(3-bromopropoxy)phenyl)propanoate (1.51 g, 5 mmol) in DMF (1 mL) was added, and the reaction mixture was left stirring at room temperature for 8 h under nitrogen. Removal of the DMF under reduced pressure gave crude product, which was dissolved in water (5 mL). Upon acidification with conc. HCl (pH approximately 2–3), a white solid began to precipitate. Digestion of the resulting solid with THF under sonication for 5–10 min provided the pure product as a white solid after filtration and washing with THF. To obtain the free base, the pH of the well-stirred suspension of the HCl salt in water was carefully adjusted with solid $NaHCO_3$ until the pH value was stable at 6. The pure free base of P218 was obtained as a white solid after filtration, washing (H_2O), and drying under reduced pressure (901 mg, 50% yield, mp = 214.5–216.5 °C); ^{1}H NMR (400 MHz, DMSO-d_6) δ: 1.01 (t, J = 7.5 Hz, 3H,), 2.17 (m, 2H), 2.33 (q, J = 7.5 Hz, 2H), 2.46 (t, J = 7.7 Hz, 2H), 2.79 (t, J = 7.7 Hz, 2H), 3.79 (t, J = 6.0 Hz, 2H), 4.16 (t, J = 6.0 Hz, 2H), 5.65 (s, 2H), 6.14 (s, 2H), 6.85 (t, J = 7.3 Hz, 1H), 6.97 (d, J = 8.1 Hz, 1H), 7.13–7.19 (m, 2H); ^{13}C NMR (100 MHz, DMSO-d_6) δ: 12.6, 23.4, 25.4, 29.5, 33.8, 64.1, 69.0, 111.3, 120.2, 127.4, 128.2, 128.7, 129.5, 156.3, 158.2, 158.9, 159.5, 174.1 ppm. HR-ESI-MS calculated for $C_{18}H_{25}N_4O_4(M+H)^+$: 361.1870, found: 361.1871.

2,4-Diamino-6-ethyl-5-(3-(2-(2-carboxyethyl)phenoxy)propoxy)pyrimidine hydrochloride (P218). One equivalent of concentrated hydrochloric acid was added to a suspension of 2,4-diamino-6-ethyl-5-(3-(2-(2-carboxyethyl)phenoxy)propoxy)pyrimidine (360.4 mg, 1 mmol) in water (1 mL). The water was completely removed under reduced pressure to give a white solid, which was digested with THF under sonication for 5–10 min. The pure product P218 was obtained upon filtration of the white solid, washing with THF, and drying under reduced pressure (377 mg, 95% yield,

mp = 194.5–195.5 °C); ^{1}H NMR (400 MHz, DMSO-d_6) δ: 1.12 (t, J = 7.5 Hz, 3H), 2.22 (m, 2H), 2.44–2.52 (m, 4H), 2.78 (t, J = 7.7 Hz, 2H), 3.89 (t, J = 6.0 Hz, 2H), 4.14 (t, J = 6.0 Hz, 2H), 6.85 (t, J = 7.4 Hz, 1H), 6.96 (d, J = 8.1 Hz, 1H), 7.14–7.19 (m, 2H), 7.50 (s, 2H), 7.84 [broad singlet (br s), 1H], 8.30 (br s, 1H), 12.11 (br s, 1H), 12.67 (br s, 1H); ^{13}C NMR (100 MHz, DMSO-d_6) δ: 11.9, 19.9, 25.4, 29.1, 33.7, 63.9, 70.8, 111.3, 120.3, 127.5, 128.7, 129.5, 147.3, 153.4, 156.2, 161.1, 173.9 ppm. HR-ESI-MS calculated for $C_{18}H_{25}N_4O_4(M - HCl + H)^+$: 361.1870, found: 361.1878.

X-ray structural studies. Recombinant PfDHFR-TS enzyme preparation and crystallization were carried out as previously reported (3). Crystals were flash-frozen in liquid nitrogen by dipping for 10 s in a corresponding crystallization solution, plus 20% glycerol as a cryoprotectant. Human DHFR was expressed and purified as described previously (4). The bound dihydrofolate was catalyzed to tetrahydrofolate upon addition of NADPH and then removed by buffer exchange with 100 mM potassium phosphate, pH 7.0, and 28 mM β-mercaptoethanol using ultrafiltration with 10 kDa Amicon. The protein was concentrated to 11 mg mL^{-1} and incubated with 2 mM each of NADPH and inhibitor on ice for 1 h prior to crystallization using the hanging drop vapor diffusion method at 295 K. Crystals were obtained from the drops of 1 μL each of the protein complex and the reservoir solution without ethanol of wells containing 100 mM potassium monohydrogenphosphate and 2.78 M ammonium sulfate supplemented with 3% (vol/vol) ethanol and then cryoprotected with Paratone-N (5). X-ray diffraction datasets were measured at 100 K at a wavelength of 1.54 Å on either a Bruker FR591 generator with a Bruker–Nonius KappaCCD detector or a Rigaku RU-H3R generator with an R-AXIS IV++ detector. Data were processed using HKL2000 suite (6) or D*TREK (7). Data processing and refinement statistics are given in Table S2. Either 1J3K or 1J3I crystal structure of PfDHFR-TS or 1HFR structure of human DHFR was used as a template in difference Fourier or molecular replacement calculations and refinement using CNS (8), or REFMAC5 (9) and MOLREP in the CCP4 suite (10, 11), along with model building with program *O* (12), and model validation using PROCHECK (13) and Moleman2 (14). Figures were prepared with PyMOL (15).

In vivo antimalarial efficacy studies. All experiments were carried out using Swiss outbred 18–20-g male CD-1 mice (Charles Rivers) kept in specific pathogen-free conditions and fed ad libitum. WR99210, P65, P218 (hydrochloride salt), and pyrimethamine (PYR; Sigma-Aldrich) were formulated for oral administration in an aqueous vehicle containing 0.5% (wt/vol) hydroxypropylmethylcellulose (HPMC), 0.4% (vol/vol) Tween 80, and 0.5% (vol/vol) benzyl alcohol (HPMC-SV) and stored at 4 °C for use within 4 d. Mice were infected intravenously with $4 \cdot 10^6$ *Plasmodium chabaudi* AS-infected red cells (day 0) obtained from infected donor mice, randomized, and divided in groups of five mice per dose level (day 0). P65, P218, and PYR were administered orally by gavage (200 μL) to *P. chabaudi* AS-infected mice once a day at the doses of 3, 1, 0.3, and 0.1 mg/kg 3 h postinfection (day 0), and on days 1, 2, and 3 postinfection, WR99210 was administered at 100, 30, 10, and 1 mg/kg. Control groups were treated with vehicle only. Parasitemias were determined by microscopic examination of Giemsa-stained thin blood films from each mouse (2 μL blood from tail vein), taken on day 4. Microscopic counts of blood films from each mouse were exported into a Microsoft Excel spreadsheet (Microsoft Corp.) and expressed as percentages of inhibition from the arithmetic mean parasitemias of each group in relation to the untreated group. Dose–response curves were obtained and ED_{50} and ED_{90} values (dose at which 50% or 90% inhibition of parasitemia is observed) and 95% CI calculated using XLFit (ID Business Solutions Ltd.), Version 4, line-fitting software using a four-parameter logistic dose–response fitting curve function.

To determine the therapeutic efficacy of P218 and PYR against *P. falciparum* V1/S in SCID mice, a "4-day test" was performed at GSK, Tres Cantos, Spain, as described previously (16). Briefly, groups of three mice engrafted with human erythrocytes were infected with 20×10^6 *P. falciparum*-infected erythrocytes per mouse. The mice were randomly assigned to their corresponding experimental groups. The treatment started at day 3 and finished at day 6 after infection. The evolution of parasitemia was assessed with samples from peripheral blood obtained at days 3, 5, and 7 after infection.

Kinetic analysis of binding characteristics. Assays were performed in 1 mL reaction mixture containing NADPH and dihydrofolate (both at 150 μM for PfDHFR assays, and both at 100 μM for hDHFR assays), 1 mg/mL BSA (for enzyme stabilization), and the inhibitor at various concentrations. The reaction was initiated by addition of the enzyme (0.7–0.9 nM for PfDHFR-WT, 1.2–1.4 nM for PfDHFR-QM, and 28–32 nM for hDHFR), and the decreasing absorbance at 340 nm was monitored until no significant change was observed. Data were fitted to Eqs. **S1**–**S3** with Kaleidagraph in order to yield the kinetic parameters:

$$A_t = A_0 - v_s t - (v_i - v_s)(1-\gamma)^* \ln\{[1 - \gamma^* \exp(-k_{obs} * t)]/(1-\gamma)\}]/(k^*_{obs}\gamma), \quad \textbf{[S1]}$$

where $\gamma = [E]^*(1 - v_s/v_i)^2/[I]$, A_t and A_0 are the absorbance at time t and time 0, v_i and v_s correspond to the initial velocity and steady-state velocity, and k_{obs} is the observed rate constant:

$$k_{obs} = k_6 + k_5[I]/(K_i^{app} + [I]), \quad \textbf{[S2]}$$

$$v_s/v_0 = 1/(1 + [I]/K_i^{*app}), \quad \textbf{[S3]}$$

where K_i^{app} and K_i^{*app} are the apparent dissociation constants for the initial enzyme-inhibitor complex (EI) and the final enzyme-inhibitor complex with conformational change (E^*I), respectively. The velocity of the uninhibited reaction (absence of inhibitor) is represented by v_0 (17).

pKa determinations. Potentiometric titrations were conducted on a Metrohm 809 Titrando autotitrator equipped with a 800 Dosino burette and were controlled by Tiamo software (Metrohm AG), Version 1.0. The pH measurements were conducted with a Metrohm LL Micro glass electrode that was calibrated on the day of use, and all titration reagents were standardized.

Titrations were conducted with WR99210 (0.3–0.5 mM) in 5–10% DMSO, P65 (0.1 mM) with 5–10% DMSO, and P218 (1 M) in 10% DMSO. Titrations were performed with potassium hydroxide and hydrochloric acid (approximately 10 mM) and titrant volume increments of 5 μL. The pH data were plotted against the equivalent volume of titrant, and the pKa value was calculated using a derivation of the Henderson–Hasselbach equation. The error in the calculated pKa value is the standard deviation of the ionization constants derived from the data points that were used.

Caco-2 permeability studies. Caco-2 cells were obtained from American Type Culture Collection and were used at passages between 31–37. Cells were seeded at a concentration of $2 \cdot 10^5$ cells/mL onto HTS-24 Transwell plates (Corning) and cultured for 21 d postseeding. Transport buffer was prepared using Hepes and HBSS. Stock solutions were prepared in transport buffer at pH 5.5 (P218) or 6.5 (WR99210 and P65) containing 1% DMSO (WR99210 and P65 only) to achieve a final concentration

of 200 μM (P218), 50 μM (WR99210), or 65 μM (P65). Compound stock solution was transferred to the apical wells while basolateral wells were filled with transport buffer at pH 7.4 containing 4% BSA (WR99210 and P65 only). Permeability studies were conducted at 37 °C with the aid of gentle mixing at 200 rpm using a microplate shaker. Samples (20 μL) were taken from the acceptor wells at regular intervals over 90 min, and donor samples were taken at 0 and 90 min for the determination of mass balance. Samples were analyzed by liquid chromatography/MS (LC/MS). Cell monolayer integrity was monitored by measurement of the transepithelial electrical resistance (TEER) and a minimum acceptance TEER value of 300 Ω/cm^2. The permeability of radiolabelled ^{14}C-mannitol was also examined in parallel studies using the same batch of Caco-2 cells to confirm monolayer integrity (P_{app} of 0.35–1.5 $\times 10^{-6}$ cm/s). The apparent permeability coefficient (P_{app}) of each compound was calculated using standard approaches (18).

Pharmacokinetic studies. Compounds were formulated for i.v. administration to rats at either 2 mg/kg (WR99210, P65, pyrimethamine) or 5 mg/kg (P218) (free base equivalent) in 5% (wt/vol) glucose containing 15 mM citrate buffer (pH 3.0) for WR99210, 20 mM citrate buffer (pH 2.5) for P65, 5% (vol/vol) DMSO for P218, or 5% (vol/vol) DMSO in 15 mM citrate buffer (pH 3.0) for pyrimethamine. Formulations were sterile filtered and a 1-mL dose volume was administered to each animal ($n = 3$ rats per compound) by i.v. infusion over 5 min via a cannula surgically inserted in the jugular vein. Oral doses of 10 (WR99210, P65, and pyrimethamine) or 30 (P218) mg/kg (free base equivalent) were prepared in a standard suspension vehicle containing either 0.5% carboxymethylcellulose (WR99210, P65, pyrimethamine) or 0.5% hydroxypropylmethylcellulose (P218), 0.4% Tween 80, and 0.5% benzyl alcohol in normal saline (WR99210, P65, pyrimethamine) or water (P218) to a final volume of 1 mL. Oral doses were administered to fasted animals ($n = 3$ rats per compound) by gavage under light anesthesia.

The same i.v. and oral formulations were used for administration of P218 to mice. Intravenous administration (5 mg/kg) was conducted via the tail vein (50 μL per mouse) and oral administration at 3 and 30 mg/kg was by gavage (100 μL per mouse).

Arterial blood samples from rats were withdrawn via a cannula surgically inserted in the carotid artery with the aid of a Culex Automated Blood Sampler instrument (Bioanalytical Systems Inc.). Blood samples (230 μL) were taken prior to dosing and at intervals up to 12–24 h following the completion of the i.v. infusion. For the oral groups, blood samples (230 μL) were taken prior to dosing and at intervals up to 24 h following oral administration. Blood samples were collected into heparinized tubes (100 IU/mL) and stored at 4 °C in the autosampler, and plasma was separated by centrifugation.

For mice, blood samples from $n = 3$ mice per time point by cardiac puncture while the animals were under gaseous isofluorane (4%) anesthesia. Blood samples were collected and processed as described for rats. Urine was not collected from mice.

Aliquots (50 μL) of plasma at each time point were taken for pharmacokinetic analysis. A blood sample (50 μL) was retained for WR99210 at each time point prior to centrifugation to obtain plasma to characterize fully both the blood and plasma concentration-time profiles. Blood (for WR99210 only) and plasma samples were stored at -20 °C until LC/MS analysis.

Noncompartmental analysis of individual rat plasma concentration-time profiles (blood concentration profiles used for WR99210 because of a very high blood-to-plasma ratio) was performed using WinNonlin Professional (Pharsight Corporation), Version 4. The terminal elimination half-life ($t^{\frac{1}{2}}$), the area under the concentration-time curves extrapolated to infinity ($AUC_{0-\infty}$), volume of distribution at steady state (V_{dss}), and clearance (CL) were calculated from individual concentration-time profiles for animals in the i.v. treatment groups. The maximum concentration (C_{max}) and the time to reach the maximum concentration (T_{max}) were taken directly from the concentration-time data for the oral treatment groups. The oral bioavailability was calculated from the ratio of the $AUC_{0-\infty}$ for each oral animal, relative to the mean $AUC_{0-\infty}$ for the i.v. treatment group normalizing for dose.

For the mouse data, doses were calculated for each animal using the individual mouse weight and the formulation concentrations. Plasma concentrations were then normalized to the target dose and averaged at each time point. Pharmacokinetic parameters were determined from the mean plasma concentration-time profiles using noncompartmental methods as described above.

LC/MS analysis. Blood and plasma samples and Caco-2 samples were analyzed using a validated LC/MS assay. Samples and calibration standards (prepared by spiking compound into blank matrix) were spiked with diazepam as an internal standard, followed by the addition of acetonitrile to precipitate proteins. Samples were vortexed and centrifuged and the supernatant analyzed by LC/MS. Analytical separations were conducted at 40 °C using either a Waters 2795 or a Waters Acquity HPLC system and either a 50 × 2-mm, 2.7-μm Supelco Ascentis Express C18 column equipped with a Phenomenex C18 Security guard column (P218) or a 50 × 2-mm, 5-μm Phenomenex Luna C8 column with a guard column of the same material (WR99210 and P65). Compounds were eluted at a flow rate of 0.4 mL/ min using a binary gradient solvent system consisting of 0.05% formic acid in water and 0.05% formic acid in acetonitrile. The acetonitrile content was varied from 2 to 95% over 3 (P218) or 5.5 (WR99210 and P65) min and the column reconditioned at the starting conditions prior to the next injection. The elution of analytes was monitored by multiple reaction monitoring in positive electrospray ionization mode using a Waters Micromass Quattro Premier or Ultima PT triple-quadrupole instrument. The capillary voltage was 3.2 kV, detector multiplier gain was 650 V, and source block and desolvation temperatures were 90 and 360 °C, respectively. The limit of quantification was 0.5 ng/mL for all analytes.

Exploratory safety studies. The hERG testing was conducted (bSYS; GmbH, Witterswil, Switzerland) using a whole-cell patch clamp technique with the hERG potassium channel stably expressed in CHO cells. The effect of P218 concentrations of 10, 30, and 100 μM on hERG-mediated tail current was assessed. An exploratory repeat-dose oral-toxicology was conducted in male Wistar rats at Harlan Laboratories SA (Barcelona). There were three treatment groups comprising 6 males each (4 animals for the main study and 2 animals for the recovery period): group 1, vehicle control; group 2, P218 100 mg/kg/*d*; and group 3, P218 300 mg/kg. The vehicle was a standard suspension vehicle containing 0.5% wt/vol hydroxypropylmethylcellulose, 0.4% vol/vol Tween 80, and 0.5% vol/vol benzyl alcohol (as a preservative). Treatments were administered once daily by oral gavage for a period of 5 d, followed by a 5-d treatment-free period. Clinical signs, food consumption, and body weights were recorded periodically during the study. On treatment day 5, blood samples were collected at 1, 4 and 24 hours post-dosing from the recovery animals to determine the plasma levels of P218. At the end of the treatment and recovery periods, hematology and biochemistry analyses and urinalyses were performed. All animals were killed, necropsied, and examined postmortem. Histological examinations were performed on an extensive set of organs and tissues from all animals under study.

1. Mamalis P, Outred DJ (1973) US Patent 3,723,429.
2. Meier C, et al. (2006) Second-generation *cyclo*sal-d4TMP pronucleotides bearing esterase-cleavable sites-the "trapping" concept. *Eur J Org Chem* 2006:197–206.
3. Chitnumsub P, et al. (2004) Characterization, crystallization and preliminary X-ray analysis of bifunctional dihydrofolate reductase-thymidylate synthase from *Plasmodium falciparum*. *Acta Cryst D* 60:780–783.
4. Kamchonwongpaisan S, et al. (2005) Stoichiometric selection of tight-binding inhibitors by wild-type and mutant forms of malarial (*Plasmodium falciparum*) dihydrofolate reductase. *Anal Chem* 77:1222–1227.
5. Cody V, Pace J, Lin L, Gangjee A (2009) The Z isomer of 2,4-diaminofuro[2,3-d]pyrimidine antifolate promotes unusual crystal packing in a human dihydrofolate reductase ternary complex. *Acta Cryst F* 65:762–766.
6. Otwinowski Z, Minor W (1997) Processing of X-ray diffraction data collected in oscillation mode. *Methods in Enzymology*, eds Carter CW Jr, Sweet RM (Academic Press, New York), pp 307–326.
7. Pflugrath JW (1999) The finer things in X-ray diffraction data collection. *Acta Cryst D* 55:1718–1725.
8. Brünger AT, et al. (1998) Crystallography and NMR system: A new software suite for macromolecular structure determination. *Acta Cryst D* 54:905–921.
9. Murshudov GN, Vagin AA, Dodson EJ (1997) Refinement of macromolecular structures by the maximum-likelihood method. *Acta Cryst D* 53:240–255.
10. Vagin A, Teplyakov A (2010) Molecular replacement with MOLREP. *Acta Cryst D* 66:22–25.
11. Collaborative Computational Project Number 4 (1994) The CCP4 suite: Programs for protein crystallography. *Acta Cryst D* 50:760–763.
12. Jones TA, Zou JY, Cowan SW, Kjeldgaard M (1991) Improved methods for building protein models in electron density maps and the location of errors in these models. *Acta Cryst A* 47:110–119.
13. Laskowski RA, MacArthur MW, Moss DS, Thornton JM (1993) PROCHECK: A program to check the stereochemical quality of protein structures. *J Appl Cryst* 26:283–291.
14. Kleywegt GJ (1997) Validation of protein models from Cα coordinates alone. *J Mol Biol* 273:371–376.
15. Schrödinger, LLC (2010) The PyMOL Molecular Graphics System, Version 1.3r1.
16. Angulo-Barturen I, et al. (2008) A murine model of falciparum-malaria by in vivo selection of competent strains in non-myelodepleted mice engrafted with human erythrocytes. *PLoS One* 3:e2252.
17. Copeland RA (2005) Evaluation of enzyme inhibitors in drug discovery. A guide for medicinal chemists and pharmacologists. *Methods of Biochemical Analysis* (Wiley, New York), Vol 46, pp 1–265.
18. Madara JL, Trier JS (1982) Structure and permeability of goblet cell tight junctions in rat small intestine. *J Membr Biol* 66:145–157.

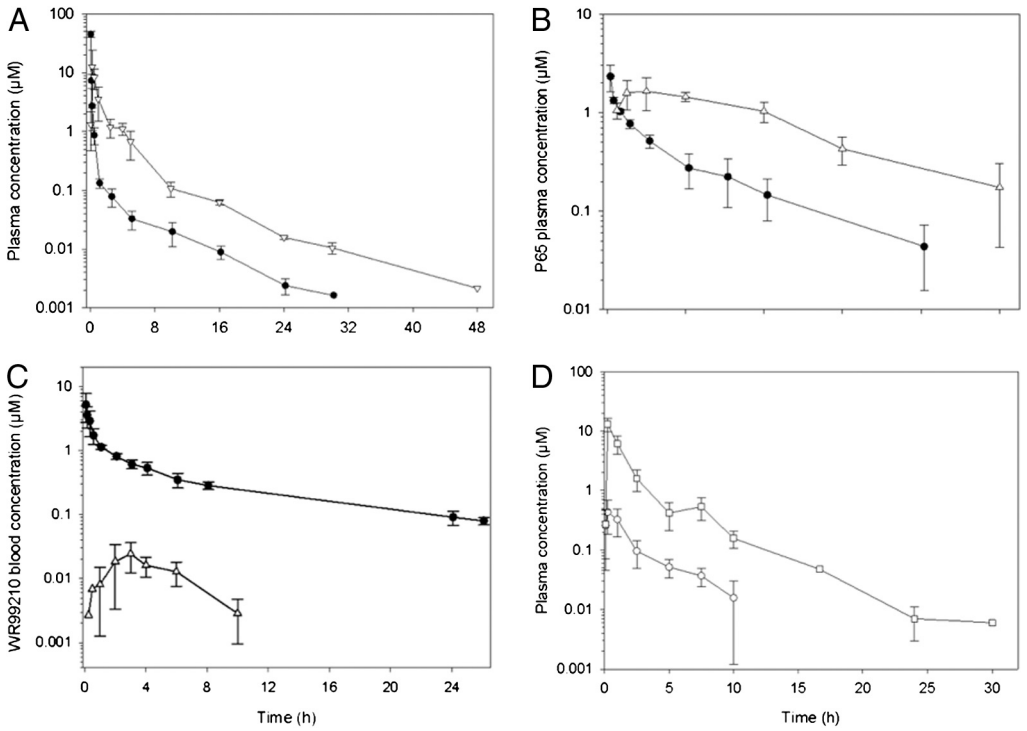

Fig. S1. Concentration-versus-time profiles for P218 (*A*), P65 (*B*), and WR99210 (*C*) after i.v. and oral administration to rats. Filled symbols represent i.v. data and open symbols represent oral data. Data represent mean ± SD ($n = 3$). Intravenous doses were 2 (P218) and 5 (P65 and WR99210) mg/kg, and oral doses were 30 (P218) and 10 (P65 and WR99210) mg/kg. (*D*) Concentration-versus-time profiles for P218 after oral administration to mice at doses of 3 (open circle) and 30 (open square) mg/kg.

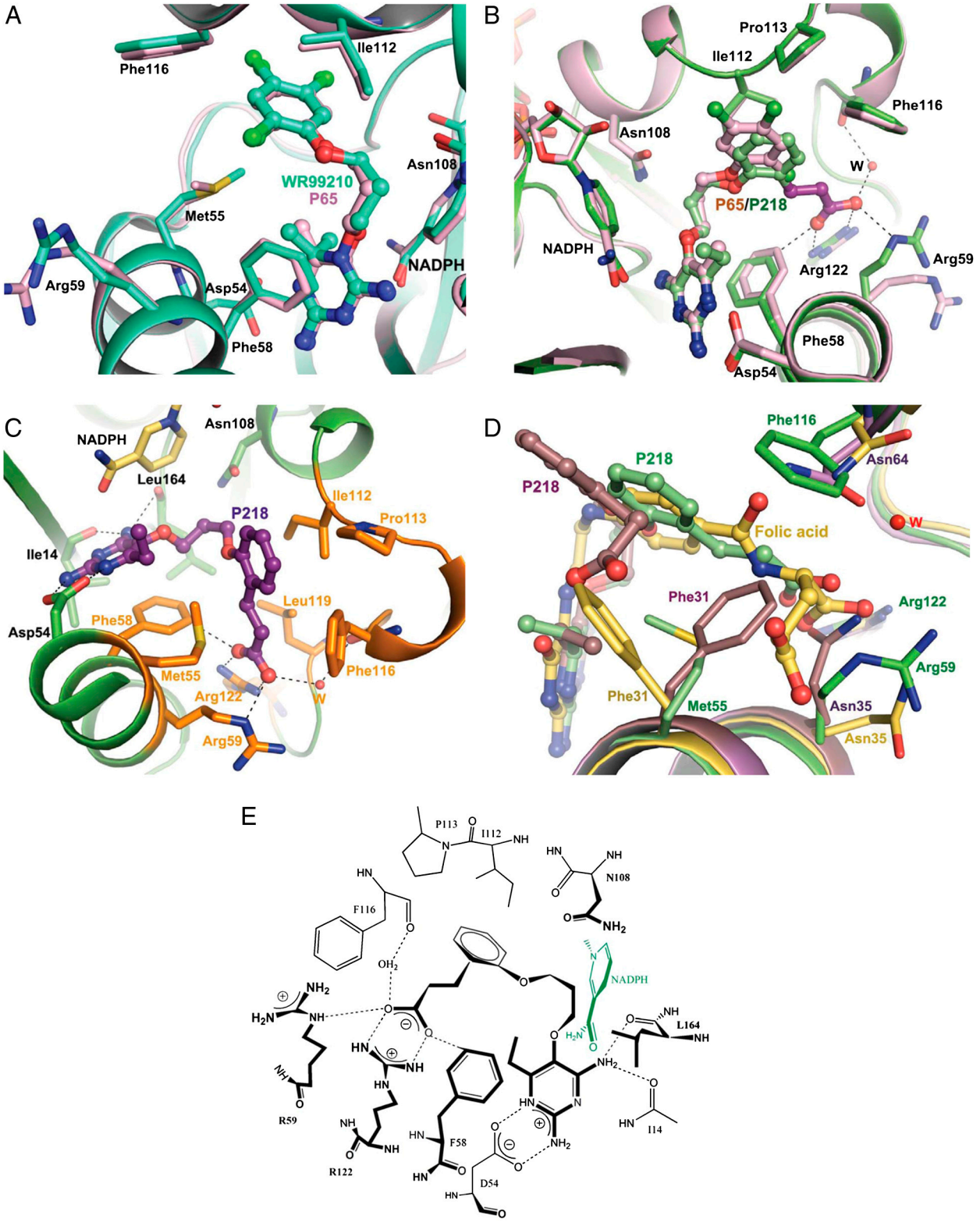

Fig. S2. (*A*) Superposition of active site regions for P65 (carbons light purple) and for WR99210 (carbons green) bound to quadruple mutant PfDHFR-TS. (*B*) Superposition of active site regions for P65 (carbons light purple) and for P218 (carbons green) bound to quadruple mutant PfDHFR-TS. Dashed lines indicate hydrogen bonds between the P218 carboxyethyl group (shown in deep purple) and Arg122, Arg59, Phe58 (CH), and an ordered water molecule (W). (*C*) P218 binding to quadruple mutant PfDHFR-TS highlighting key protein residues (carbons, orange) that interact with the inhibitor's carboxyethylphenyl group. Dashed lines indicate hydrogen bonds. (*D*) Superposition of active site regions for P218 bound to quadruple mutant PfDHFR-TS (green) and human DHFR (light purple). Also shown is the structure of human DHFR with bound folic acid (yellow, PDB ID code 2W3M) in the same orientation. From this, one can see how P218 would fit into human DHFR if it binds in the same manner as it does to quadruple mutant PfDHFR-TS, but because of three nonhomologous amino acid substitutions in the vicinity of Arg122 (PfDHFR-TS numbering), P218 binds differently to the human and malarial enzymes. (*E*) A line diagram showing some of the important interactions between P218 and the active-site residues of the quadruple mutant PfDHFR. Hydrogen bonds are indicated with dotted lines.

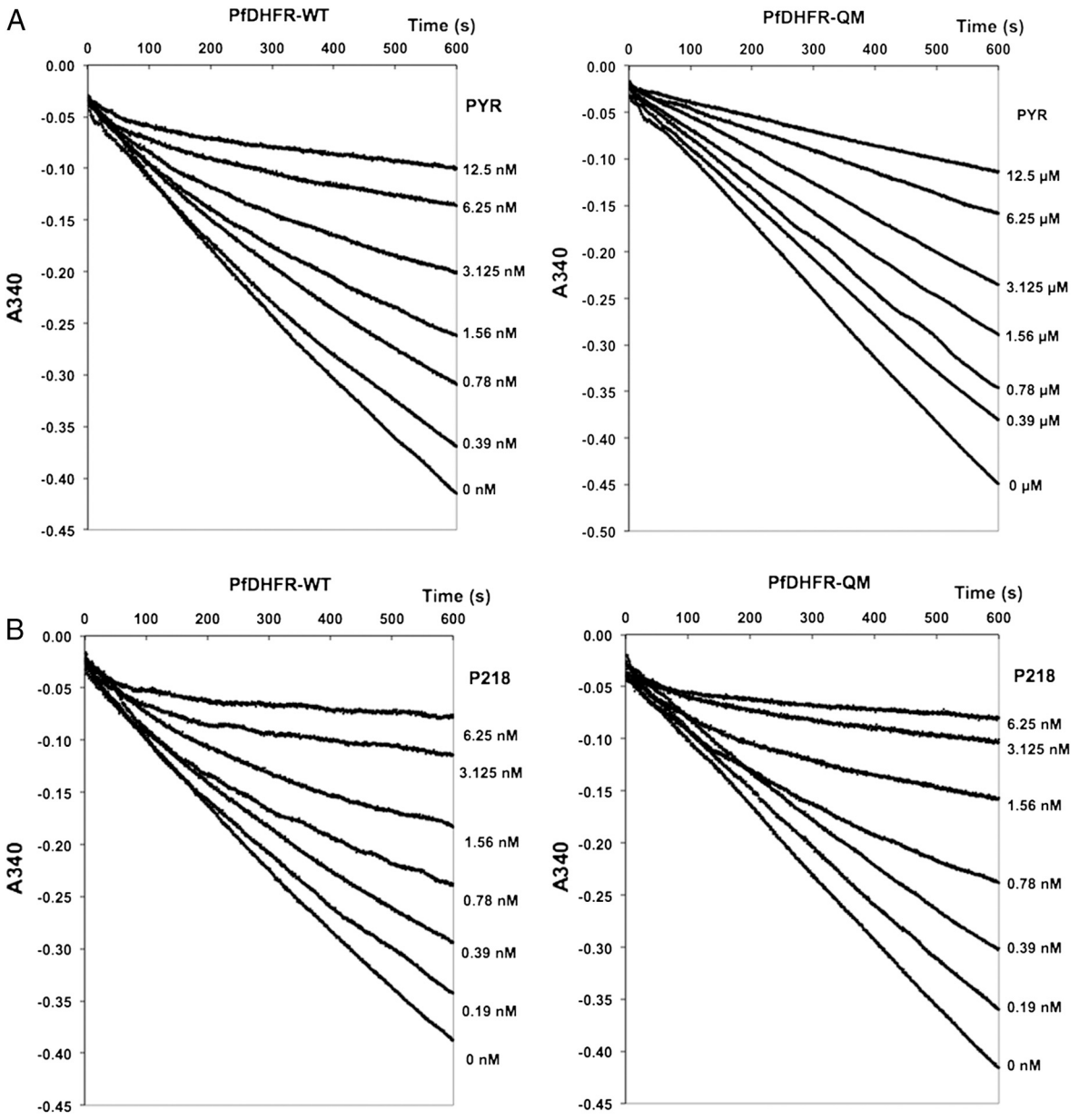

Fig. S3. Slow onset of tight binding of DHFR inhibitors. (*A*) PYR binding with wild-type (PfDHFR-WT) and quadruple mutant (PfDHFR-QM) enzyme; (*B*) P218 binding with PfDHFR-WT and PfDHFR-QM. Progress curves were analyzed as in *Materials and Methods*, yielding the kinetic data in Table 2.

Table S1. Pharmacokinetic properties for P218, P65, and WR99210 after i.v. and oral administration to rats and mice

Compound ID	Rats*			Mice†
	P218	P65	WR99210‡	P218
Intravenous half-life (h)	7.5 ± 2.4	2.3 ± 5	7.5 ± 2.0	4.8
CL (mL/ min /kg)	39.9 ± 4.5	44.2 ± 17.3	8.8 ± 0.7	43.6
V_{dss} (L/kg)	2.1 ± 0.5	8.3 ± 2.1	7.1 ± 1.0	2.5
Oral C_{max} (μM)	15.8 ± 9.9	1.8 ± 0.5	0.03 ± 0.01	0.43¶/13.2‖
Oral T_{max} (h)§	0.5	2	1	0.25¶, ‖
Oral half-life (h)	7.3 ± 1.6	4.9 ± 1.3	c.n.c.	c.n.c.¶/4.0‖
Oral bioavailability (%)	46.3 ± 11.4	82.6 ± 21	<1	c.n.c.¶/62.0‖

c.n.c., Could not calculate.
*Mean ± SD for $n = 3$.
†Based on mean data.
‡Data based on whole-blood profiles because of a very high blood-to-plasma ratio for this compound.
§Median.
¶3 mg/kg.
‖30 mg/kg.

Table S2. Data collection and refinement statistics for liganded PfDHFR-TS and hDHFR

	QM DHFR-TS		WT DHFR-TS	hDHFR
Ligands	P218, NADPH	P65, NADPH	DHF, NADP+, dUMP	P218, NADPH
Wavelength (Å)	1.54	1.54	1.54	1.54
Space group	$P2_12_12_1$	$P2_12_12_1$	$P2_12_12_1$	$H3$
Cell parameters, *a*, *b*, *c* (Å)	58.50, 156.20, 164.59	57.95, 156.45, 164.65	58.06, 156.78, 165.03	85.28, 85.28, 77.13
Resolution (Å)	50–2.40 (2.49–2.40)	51.79–2.38 (2.47–2.38)	50–2.50 (2.59–2.50)	33.31–2.05 (2.12–2.05)
Measured/unique reflections	213,512/57,640	193,382/60,475	309,667/53,137	41,284/13,122
Completeness (%), overall/highest shell	96.5/86.7	95.9/95.8	100/99.8	95.1/95.1
$\langle I/\sigma I\rangle$, overall/highest shell	20.5/3.5	6.9/2.0	19.1/2.8	5.2/1.8
R_{merge}* (%), overall/highest shell	4.7/24.8	5.5/29.0	9.0/49.0	7.0/24.4
Molecules/ASU	2	2	2	1
Wilson B factor (Å^2)	45.8	49.8	47.8	27.0
R_{factor}†/R_{free}‡ (%)	20.5/23.9	21.7/28.2	21.0/26.2	20.5/24.9
Rmsd				
Bond length (Å)	0.007	0.014	0.009	0.007
Bond angles (°)	1.333	1.461	1.317	1.377
Ramachandran plot (%)				
Favored regions	85.7	87.1	89.3	90.6
Allowed regions	14.2	12.9	10.4	9.4
Outliers	0.1	0.0	0.3	0.0

*$R_{merge} = (\Sigma h \Sigma i |I(h, i) - \langle I(h)\rangle|)/\Sigma h \Sigma i |I(h, i)|$, where $I(h, i)$ is the intensity of the ith measurement of reflection h, and $\langle I(h)\rangle$ is the mean intensity of $I(h, i)$ for all i measurements.
†$R_{factor} = \Sigma hkl||F_o| - |F_c||/\Sigma|F_o|$, where F_o is the observed structure-factor amplitude, and the F_c is the structure-factor amplitude calculated from the model.
‡R_{free} is the same as R_{free} except calculated from 5% data excluded from refinement.